Modulation of Aβ aggregation by Aβ-derived fragment peptide: A molecular dynamics study

A

Dissertation submitted

in partial fulfilment of the requirements for the degree of

Master of Science

in

Chemistry

By

Mehak Aggarwal

(Reg. No: 302102010)

Under the guidance of

Dr. Bhupesh Goyal

SCHOOL OF CHEMISTRY AND BIOCHEMISTRY

THAPAR INSTITUTE OF ENGINEERING AND TECHNOLOGY, PATIALA–147004

JULY, 2023

DECLARATION

I hereby, declare that the dissertation entitled, "**Modulation of Aβ aggregation by Aβ-derived fragment peptide: A molecular dynamics study**" presented in partial fulfilment of the requirements for theaward of the degree of **Master of Science in Chemistry** to **School of Chemistry and Biochemistry, Thapar Institute of Engineering and Technology, Patiala** is a record of the independent research conducted by me from January to July 2023 under the guidance of **Dr. Bhupesh Goyal**. Additionally, none of the components of this dissertation have been submittedto another university for consideration of a different degree or diploma.

Signature of Candidate
Mehak Aggarwal

Date: 17 July, 2023

Place: TIET, Patiala Regn. No. 302102010

CERTIFICATE

This is to certify that the dissertation entitled **"Modulation of Aβ aggregation by Aβ-derived fragment peptide: A molecular dynamics study"** being submitted by **Ms. Mehak Aggarwal** to **School of Chemistry and Biochemistry, Thapar Institute of Engineering and Technology, Patiala** inpartial fulfillment of the requirements for the award of degree of **Master of Science in Chemistry,** is an authentic record of the work carried out by the candidate under my/our guidance and supervision. She has fulfilled the requirements for the submission of this dissertation, which to my knowledge has reached the requisite standard. The results embodied in the dissertation have not been submitted in part or full to any other University or Institute for the award of any other degree or diploma.

Date: 17 July, 2023

Place: TIET, Patiala

Bhupesh Goyal

Signature

Mehak Aggarwal

Signature of the candidate

Dr. Bhupesh Goyal

Assistant Professor

School of Chemistry and Biochemistry

ACKNOWLEDGEMENT

First and foremost, I express my gratitude to the Almighty God, whose countless blessings, knowledge, and opportunities have enabled me to successfully complete my dissertation. I extend my heartfelt thanks to Dr. Satnam Singh, Professor and Head of the School of Chemistry & Biochemistry, for granting me the opportunity to immerse myself in the world of research through this dissertation.

I am sincerely thankful to my supervisor, Dr. Bhupesh Goyal, for their exceptional guidance, expertise, and unwavering support throughout the entire research process. Their insights and suggestions have been instrumental in shaping this thesis, and I am truly grateful for their mentorship.

I would also like to express my profound appreciation to Ms. Diksha, my mentor for guiding me throughout and supporting me endlessly. This work would not have been possible without her constant guidance. I would also like to thank all my lab mates, Ms. Arushi, Ms. Anisha, Ms. Tanishka, Ms. Gurmeet, Mr. Ishwar and Mrs. Apneet Kaur for encouraging and helping me throughout my project.

In this cherished pursuit, my family has been my guiding light. To my parents, Mr. Rajinder Kumar and Mrs. Renu Aggarwal, your unwavering love and guidance have been my inspiration in all endeavors. You are my ultimate role models. A special thanks to my sister, Navya, for her unending support, which has lifted me through every challenge. Your presence has made this journey truly beautiful.

My heartfelt thanks go out to Thapar Institute of Engineering and Technology (TIET) for providing the necessary facilities and infrastructure that allowed me to carry out this study. In conclusion, the completion of this thesis is a result of the collaborative efforts and support of an exceptional network of individuals, and for that, I am genuinely thankful.

Thank you all.

Mehak Aggarwal

Date: 17 July, 2023

Place: TIET, Patiala. Mehak Aggarwal

ABSTRACT

The self–aggregation of amyloid-β ($A\beta_{42}$) into β–sheets is considered to be responsible for the onset of Alzheimer's Disease (AD), a neurodegenerative disease with no clinically accepted treatment. The N–terminal ($^{16}KLVFF^{20}$) is identified as a self–recognition region and the central hydrophobic core (CHC) which is crucial for the formation and stabilization of the β– sheets. Mallesh et al. have recently reported KLLFF, produced by single point mutation by replacing Val18 in KLVFF with leucine KLLFF as a potential inhibitor against Aβ aggregation. The mechanism by which KLLFF hinders Aβ aggregation remains an enigma. To gain insightsinto this inhibitory mechanism, molecular dynamics (MD) simulations have been performed. The molecular docking was performed using AutoDock Vina which predicted a favourable binding energy of –5.2 kcal/mol for $A\beta_{42}$–KLLFF complex. The MDsimulations depicted enhanced structural stability for $A\beta_{42}$ in the presence of KLLFF. The presence of KLLFF remarkably prevented the β–sheet formation by reducing the side–chain contacts at the C– terminal, Gly33–Val40 of $A\beta_{42}$. According to the per residue binding energy Phe4, Arg5, Val12, His13, Val18 and Phe19 contributed maximum to binding of $A\beta_{42}$ with KLLFF. KLLFFfurther reduced the intramolecular hydrogen bonds of $A\beta_{42}$, therebystabilizing the native of structure $A\beta_{42}$. Understanding the inhibitory mechanism of KLLFF against $A\beta_{42}$ holds great promise for the development of potent drugs to combat AD. Such insights could pave the way for more effective treatments against AD.

TABLE OF CONTENTS

LIST OF TABLES

LIST OF FIGURES

LIST OF ABBREVIATIONS

Abbreviations	Full meaning/name
AD	Alzheimer's Disease
PD	Parkinson's Disease
ALS	Amytrophic lateral sclerosis
Aβ	Amyloid Beta
APP	Amyloid Precursor Protein
CHC	Central Hydrophobic Core
NT	N – Terminal
FTIR	Fourier Transform Infrared
ThT	Thioflavin T
CDP	Cyclic Dipeptide
AFM	Atomic force microscopy
MD	Molecular Dynamics
PDB	Protein Data Bank
RMSD	Root Mean Square Deviation
RMSF	Root Mean Square Fluctuations
R_g	Radius of Gyration
DSSP	Dictionary of the Secondary Structure of Proteins
MM–PBSA	Molecular Mechanics Poisson Boltzmann Surface Area

CHAPTER 1: Introduction

1. Introduction

Proteins are macromolecules which serves as building blocks of living systems due to their vital activities in enzymes, cytoskeleton, muscles, and hormones.[1] The proper three–dimensional structures of proteins in their folded, mature forms are essential for their proper functioning.[2] However, any alterations in the protein structure during the intricate process of protein folding results in misfolding and subsequent aggregation.[3] The pathology of several neurodegenerative disorders, such as Alzheimer's disease (AD), Huntington's disease, frontotemporal dementia, Parkinson's disease (PD), and amyotrophic lateral sclerosis (ALS), involves the self–association of misfolded proteins into aggregates.[4,5] Among all theneurodegenerative diseases, AD is the most common form of the dementia that is prevalent without a cure.[6] The symptoms include progressive deterioration of memory, cognitive function,and physical abilities.[7] The global population affected by AD comprises approximately 55 millionindividuals, while the incidence of dementia continues to escalate at a rapid pace. The global economic for treatment of dementia was estimated at around $355 billion in 2021 and is projectedto surge to an astounding $1.1 trillion by the year 2050.[8,9]

The accumulation of amyloid-β (Aβ) protein which comprises of 39 or 42 amino acid residues is majorly responsible for the pathology of AD.[10,11] The initial step in the formation of Aβ involves the sequential proteolytic cleavage of a transmembrane precursor protein (APP) by enzymes β– and γ–secretases.[12] Aβ is known to have two structural variants $A\beta_{40}$ and $A\beta_{42}$[13] however, $A\beta_{40}$ is the more abundant alloform than $A\beta_{42}$. Although, $A\beta_{42}$ is believed to be more neurotoxic and majorly responsible for aggregation.[14] Under normal physiological conditions the Aβ readily undergoes self–aggregation, forming the β-sheets that are transformed into insoluble aggregates, oligomers and protofibrils which subsequently forms neuritic plaques.[15]

Several inhibitors that can hinder the aggregation of Aβ molecules or disrupt pre-existing Aβ aggregates have acquired significant interest as promising drug candidates for AD.[16,17] These compounds include inhibitors like peptides[18], surfactants[19], small molecules[20] andnanoparticles[21]. The strategies for the inhibition of aggregation include blocking the expression of APP, inhibiting the cleavage of APP, or targeting the aggregation of Aβ against the Aβ aggregation.[22,23]

The characteristics of peptide–based inhibitors that makes them particularly advantageous in inhibiting the aggregation process over other inhibitors are their bio–compatibility, enhanced ability to cross blood brain barrier, increased selectivity and less toxicity.[24] Peptide sequence

derived from $A\beta_{42}$ sequence like $A\beta_{15-22}$, $A\beta_{16-23,}$ and $A\beta_{17-22}$ bind to the complementary parent sequences due to their self–recognition property, and inhibit the self–aggregation by blocking the binding sites of $A\beta_{42}$.[25,26] The central hydrophobic core (CHC) region being the self–recognition region comprises the N–terminus fragment 16KLVFF20 which is believed to drive the process of aggregation.[27] Various researchers have confirmed that the peptides derived from the parent sequence could not efficiently inhibit the aggregation process, thus novel peptides with several modifications are being designed been to weaken the aggregation process.[28]

Mallesh et al. investigated the impact of a single amino acid mutation in the N–terminal (NT) region of the $A\beta_{42}$ peptide, specifically inducing β–sheet formation.[29] The authors designed 14 hydrophobic peptides (NT–01 to NT–14) by substituting the V18 with hydrophobic residues like leucine and proline in the original $A\beta_{42}$ peptide fragment (KLVFFAE). Among the 14 peptides tested, NT–02 (KLLFFA), NT–03 (KLLFF), and NT–13(LPFFAE) showed significant influence on $A\beta_{42}$ aggregate formation. When these NT peptides were co–incubated with the $A\beta_{42}$ peptide, they caused a notable reduction in β–sheet formation and an increase in the random coil content of $A\beta_{42}$ which was confirmed through circular dichroism (CD) spectroscopy and Fourier transform infrared spectroscopy (FTIR). Furthermore, the reduction in fibril formation was measured using the thioflavin–T (ThT) binding assay. ThT Assay highlighted that NT–03 showed inhibition of 54.26% at 5μM when treated with $A\beta_{42}$. The inhibition of aggregation was also assessed through Congo red and ThT staining techniques, as well as electron microscopy examination. The analyses supported the observation that the NT–03 peptide had the ability to impede fibril formation. Additionally, the NT–03 peptide increased the cell viability to 92.41% exhibiting a protective effect on PC–12 differentiated neurons against $A\beta_{42}$–induced toxicity and apoptosis when tested *in vitro*. Despite the extensive studies, the molecular mechanism behind the inhibitory potential of KLLFF has not been discovered yet. In this regard, MD simulations for two different systems $A\beta_{42}$ and $A\beta_{42}$ + KLLFF have been employed to understand the interactions between $A\beta_{42}$ and KLLFF and the molecular mechanism of inhibition of aggregation.

CHAPTER 2: Literature Review

In 2022, Konar et al., conducted a study where they designed and synthesized a series of $A\beta_{14-23}$ peptidomimetics by incorporating cyclo (Lys–Asp) based cyclic dipeptide (CDP)–unnatural amino acid (kd) at three different positions.[30] The objective was to investigate the impact of these peptidomimetics on the aggregation of Aβ at pH 7.4 and 2.0. Among the synthesized peptidomimetics Akd^{NMC} (V) which contained the CDP unit at the N– terminal, C–terminal and at the middle exhibited the most effective inhibition. The molecular docking was performed and Akd^{NMC} revealed a binding energy of –5.3 kcal/mol. ThT Assay was performed and it was found that Akd^{NMC} had the longest lag time (t_{lag}) 316.8 hour at pH 7.4. CD studies indicated that at pH7.4 two negative peaks appeared at 200 nm and 210 nm suggesting a reduction in β–sheet. FTIR studies of $A\beta_{14-23}$ incubated with Akd^{NMC} (V) showed a peak at 1640 cm^{-1} and 1670 cm^{-1} and 1660 cm^{-1} for random coil and α–helix, respectively. AFM imaging further confirmed the inhibition of aggregation. Cytotoxicity assay demonstrated that $A\beta_{14-23}$+ Akd^{NMC} displayed a cell viability rateof 99%. Further, molecular docking was performed between $A\beta_{14-23}$ and Akd^{NMC} and revealed a binding energy of –5.3 kcal/mol. The findings indicated that $A\beta_{14-23}$ + Akd^{NMC} was a potential inhibitor at pH 7.4.

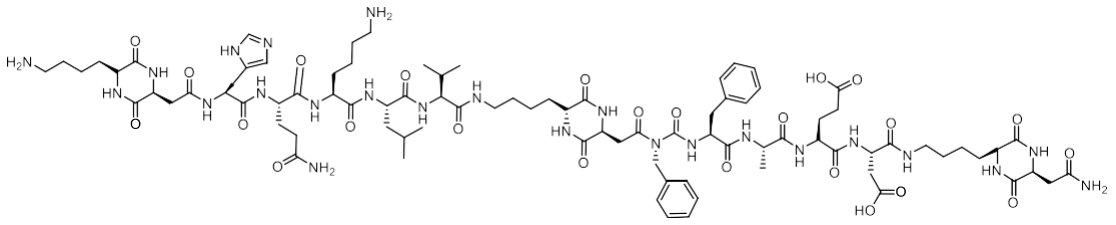

Fig. 1 Structure of $A\beta_{14-23}$ + Akd^{NMC}

In 2022, Kundal and co–workers, investigated a small library of novel peptides via MD simulations to assess their interactions with the $A\beta_{42}$ (PDB ID: lIYT).[31] The peptides were designedbased onthe amyloidogenic region (Lys16–Ala21) and were subjected to one/two–point mutationto enhance the inhibition tendency and to increase the stability of $A\beta_{42}$ against enzymatic degradation. Docking results revealed that the peptide DKAPFF (P12) showed the highest bindingenergy of –70.17 kcal/mol with $A\beta_{42}$. The residues of $A\beta_{42}$ involved in hydrogen bonding with P12included, Ala21, Lys28, Gly38, Ala42 whereas Ala42 and Lys28 were involved in hydrophobic contacts. The conformational changes in the structure of $A\beta_{42}$were analysed by RMSD, RMSF and

R_g. It was observed that in the presence of P12 RMSD value decreased from 1.35 nm to 0.7 nm and RMSF analysis showed lesser fluctuations R_g value decreased from 2nm to 1.09 nm. Further the analysis of hydrogen bonds revealed a decrease in the intramolecular hydrogen bonds of $A\beta_{42}$ on incorporation of P12. All these analyses indicated a more stable structure of $A\beta_{42}$ in the presence of P12. The information gained can be used to explore P12 as a therapeutic agent againstAD.

Fig. 2 Structure of P12 (DKAPFF)

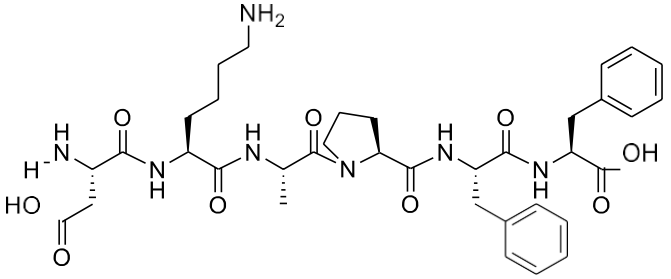

In 2021 Liu et al., elucidated the influence of chirality of the heptapeptide LVFFARK (LK7) on $A\beta_{42}$ protein. The effects of L–LK7 and D–LK7 enantiomers on Aβ were compared.[32] It was observed that both the enantiomers were capable of inhibiting the aggregation but the D–enantiomer was preferred as it exhibited the stronger inhibition, which was proven by lower fluorescence intensity of 18% for D–LK7 in the ThT assay and absence of almost no $A\beta_{42}$ aggregates in the AFM imaging. The results of the CD spectroscopy revealed a reduction of β–sheet from 47.6% to 20.4% for the D–enantiomer. MTT cell viability demonstrated that the cell viability for D–LK7 was increased to 83%. Molecular docking utilizing AutoDock Vina was used to gain insight into the molecular mechanisms. The binding energy of D– LK7 was observed –4.4kcal/mol, lower than L–LK7. These results highlighted the impact of chirality on Aβ aggregation and opened paths for the design of the new inhibitors.

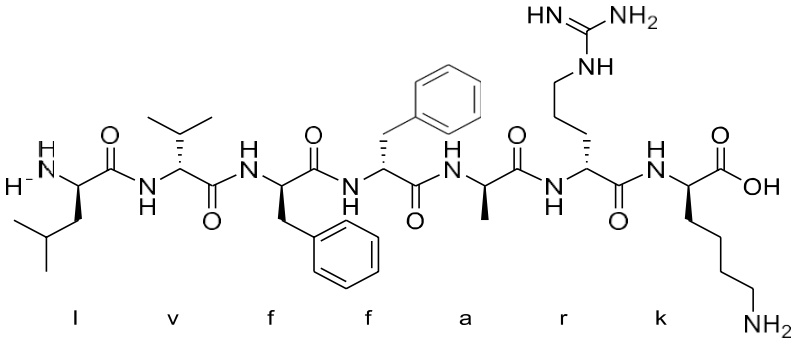

Fig. 3 The molecular structure of D–LVFFARK.

In 2021, Wang et al.[33] synthesized a zwitterionic polymer with short dimethyl side chains (denoted by pID) and conjugated it with LK7 peptide inhibitor for better inhibition against Aβ42 aggregation. Interesting and unexpected property of LK7@pID (Ac-LVFFARK-NH2) conjugate was revealed by mechanistic studies, i.e., the effective elimination of AB induced cytotoxicity despite forming more fibrils when compared with Aβ42-alone system. Primarily, the hydrophobic interactions between Aβ42 molecules and LK7@pID were formed which triggered Aβ42 aggregation initially by promoting the hydrophobic environment within assembled micelles of LK7@pID. Furthermore, in the aggregation process, LK7@pID micelles were pushed apart by intense contacts with AB, resulting in hybrid and heterogeneous fibrillar aggregates that differed from typical Aβ42 fibrils. This is a unique Trojan horse- like property of LK7@pID conjugates which has not been observed for other inhibitors previously. Therefore, these finding breaks through the traditional amyloid modulator design ideas and offers new views for modulating amyloid protein aggregations.

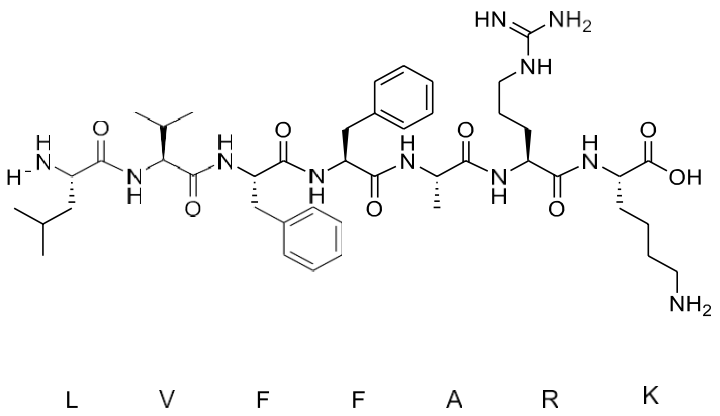

Fig. 4 The molecular structure of LVFFARK.

In 2020 Horsley and colleagues, designed a hexapeptide, that incorporated a recognition component (KLVFF) and a β–sheet disruption element (Aib).[34] This was the first study to exploit thesynergy between a recognition and disruption component. The hexapeptide referred as peptide 2 exclusively comprised of D–amino acids, to enhance the specificity towards $A\beta_{42}$. Various analyses including the Fluorescence assay, native ion mobility (IM–MS) and cell viability assay, collectively demonstrated the highly specific interaction between $A\beta_{42}$ and the peptide. Additionally, ThT Assay revealed that the designed peptide completely inhibited β– sheet formation at a molar ratio of 1:2. Cell viability assay did not indicate any cytotoxic effect whenthe peptide 2 was incubated with $A\beta_{42}$ in 2:1 molar ratio. The successful utilization of synergism between the recognition and the disrupting components in this study provides a promising strategy to design anti–amyloid drugs.

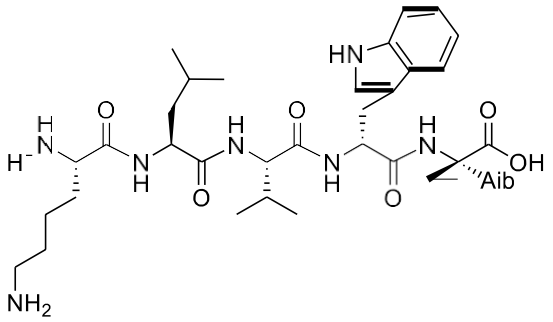

Fig. 5 The Structure of D–isoform of the designed peptide.

In 2019, Mondal et al.,[35] implemented a pharmacophore based in silico analysis of known neuroprotective molecules to identify a short hexapeptide "LETVNQ" (LE6) as shown in Fig. 6, that prevents Aβ aggregation, neurotoxicity and also provides a stability to intercellular tubulin. Several experimental results suggested that LE6 promote neurite outgrowth and has no cytotoxic effect for differentiated PC12 neurons. LE6 enhanced the rate of polymerization of intracellular microtubules, thus, balancing the complex microtubule network in cells. Further, substantial stability of LE6 in human serum (~35% stable after 24 h) makes this short hexapeptide a potent candidate against AD.

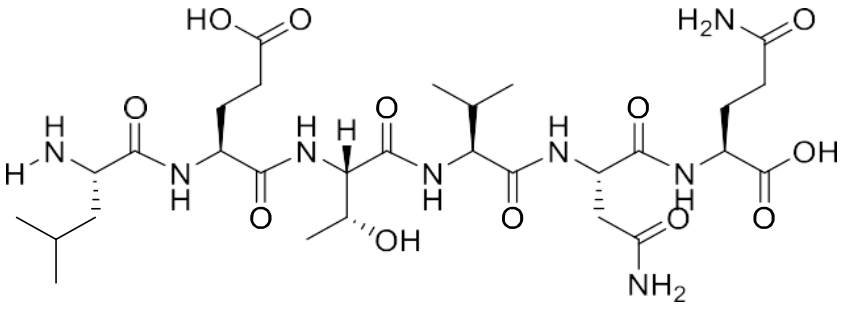

Fig. 6 The molecular structure of LETVNQ.

CHAPTER 3: Computational Details

3.1 Protein and Ligand preparation

The primary amino acid sequence of the $A\beta_{42}$ monomer contains 42 amino acids ($D_1AEFRHDDSGY_{10}EVHHQKLVFF_{20}AEDVGSNKGA_{30}IIGLMVGGVV_{40}IA$). The structure of the full–length $A\beta_{42}$ monomer (PDB ID: lIYT)[36] was obtained from the RCSB Protein Data Bank[37] (Fig. 2a). ChemDraw Professional 15.0[38] was used to draw the structure of the peptide KLLFF. The N– terminal and C–terminal of KLLFF was kept amidated. Chem 3D ultra was used for energy minimization (Fig. 2b). The PDBQT files were obtained using the AutoDock Tools 1.5.6 software.[39]

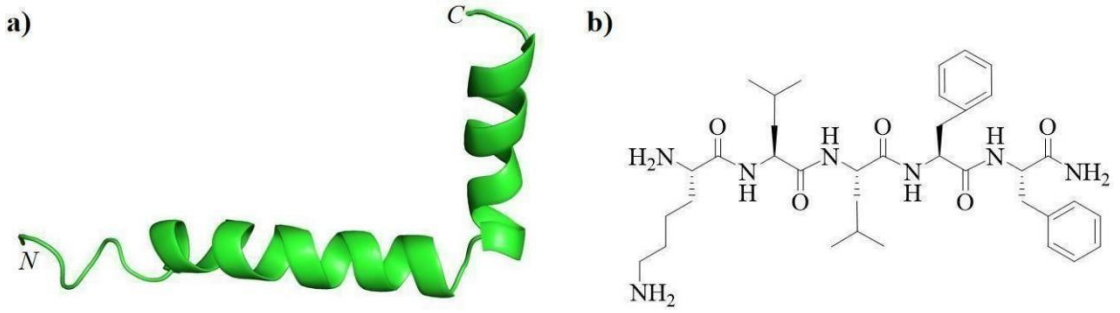

Fig. 7. a) The 2D structure of $A\beta_{42}$ (PDB ID: 1IYT) b) The chemical structure of the peptide NH_2–KLLFF–NH_2.

3.2 Molecular Docking

The molecular docking was conducted using AutoDock Vina[40] to assess the binding pose of KLLFF with Aβ42. The PDBQT files for $A\beta_{42}$ and $A\beta_{42}$–KLLFF were generated using AutoDock tools. For the docking study, the $A\beta_{42}$– KLLFF complex was enclosed within agrid box. The grid spacing was set at the value of 1.00Å, and the dimensions of the grid box were set to 38 × 30 × 53 Å. The center of the grid was positioned at x = –4.019, y = –0.009, and z = –2.294. In the case of $A\beta_{42}$, Kollman charges were added along with polar hydrogens. The resulting interactionsbetween $A\beta_{42}$ and KLLFF were analyzed using PyMOL and ligplot$^+$ software.[41] The docking analysis provided insights into the specific interactions between $A\beta_{42}$ and KLLFF which allowedfor further examination.

3.3 System preparation for Molecular dynamics simulations

To study the dynamic behaviour of $A\beta_{42}$ in the presence and absence of KLLFF, MD simulations[42] were performed using the GROMACS[43] program with the Amber99SB–ILDN force field[44]. Two independent systems were considered: $A\beta_{42}$ (alone) and the $A\beta_{42}$–KLLFF (complex). The cubic boxes with dimensions of 7.36 nm × 7.36 nm × 7.36 nm were created and the systems were solvated using the TIP3P water model[45]. To neutralize the charge of $A\beta_{42}$ (–3)[46],3 Na+ ions were added. Additionally, 0.15M NaCl was included in the systems to mimic the physiologicalconditions. The $A\beta_{42}$ system contained 12,682 water molecules, while the $A\beta_{42}$–KLLFF system contained 12,513 water molecules (Table 1). The equilibration process started with NVT equilibration (constant number of particles, volume, and temperature) using Berendsen thermostat[47] for 500 ps at 300 K. This was followed by NPT (constant number of particles, pressure, and temperature) equilibration coupled with Parinello–Rahman barostat[48] for an additional 500 ps. The constraint algorithm LINCS[49] was used for bond lengths. The smooth particle–mesh Edwald summation method[50] was used to calculate long–range interactions. MD trajectories generated from the simulations for both systems were analysed using GROMACS toolsand PyMOL software. The analyses allowed for the examination of the dynamics, interactions, and structural stability of the systems throughout the simulation time.

Table 1. Details of MD simulated systems.

System	Simulation time (ns)[b]	Box dimensions (nm^3)	Number of water molecules in box
$A\beta_{42}$	50	7.36 × 7.36 × 7.36	12682
$A\beta_{42}$ + KLLFF	50	7.36 × 7.36 × 7.36	12513

[a]$A\beta_{42}$ (PDB ID: 1IYT), [b] The Amber99SB–ILDN force field and TIP3P water model are used for simulations.

3.4 Structural analysis details

The structural stability of both the $A\beta_{42}$ peptide and the $A\beta_{42}$–KLLFF complex was analyzed using various tools provided by GROMACS. The gmx_rms tool was employed to calculate the Root Mean Square Deviation (RMSD), which measures the overall structural deviation of the backbone atoms for $A\beta_{42}$ peptide and $A\beta_{42}$–KLLFF complex from their initial conformations throughout the MD simulation. The gmx_rmsf tool was used to calculate the Root Mean Square Fluctuation (RMSF), which quantifies the flexibility of each residue in the $A\beta_{42}$ peptide or $A\beta_{42}$–KLLFF complex during the MD simulation. The gmx_gyrate tool was employed to calculate the R_g (Radius of Gyration), which provides a measure of the compactness of the $A\beta_{42}$ during the MD simulation. The gmx_sasa tool was used to evaluate the Solvent Accessibility Surface Area (SASA). The

gmx_hbond tool was utilized to calculate hydrogen bonds. The bond angle and hydrogen bond length during hydrogen bond analysis were kept at default. The secondary structure details for both systems were evaluated using do_dssp tool[51] of GROMACS. Additionally, gmx_mindist was employed to analyze the side–chain contacts of $A\beta_{42}$ in the presence and absence of KLLFF during the MD simulation.

3.5 Binding free energy calculations by MM–PBSA

The Molecular Mechanics Poisson Boltzmann Surface Area (MM–PBSA) method was used to estimate the total binding free energy of $A\beta_{42}$ to KLLFF. The binding free energy was calculated using the g_mmpbsa tool.[52] The binding free energy was calculated as per the following equations:

$$\Delta G_{Binding} = \Delta E_{MM} + \Delta G_{solv.}$$

where, ΔE_{MM} and ΔG_{solv} terms denotes the molecular mechanics energy and the solvation energy term. ΔE_{MM} is calculated as the sum of the van der Waals energy (ΔE_{vdw}) and the electrostatic energy (ΔE_{elec}). $\Delta G_{solv.}$ is calculated as the sum of the polar solvation energy (ΔG_{ps}) and non–polar solvation energy (ΔG_{nps}). The contribution of each residue in binding free energy were estimated by MmPbSaDecomp.py python script.

CHAPTER 4: Results and Discussion

Recently in 2023, Mallesh et al. designed a hydrophobic peptide, NT–03 (KLLFF) by mutating Val18 in KLVFF with hydrophobic leucine.[29] Extensive biophysical studies highlighted that KLLFF significantly inhibited the aggregate formation of $A\beta_{42}$. However, the inhibitory mechanism of KLLFF against $A\beta_{42}$ aggregation remains obscure. In this work, MD simulations have been employed to understand the interactions between $A\beta_{42}$ and KLLFF and the molecular mechanism of inhibition of aggregation.

4.1 Molecular docking studies and key interactions of KLLFF with $A\beta_{42}$.

The results of the molecular docking revealed the favourable binding energy of –5.2 kcal/molfor the interaction of $A\beta_{42}$ and KLLFF. The binding of KLLFF peptide resulted in the formation of four hydrogen bonds with residues Glu11 and Gln15 of $A\beta_{42}$ (Fig. 3a, Table 2). The docking results are consistent with the previous study reported by Biswas et al. in which peptide (NAVSIQ) formed hydrogen bonds with Glu11 and Gln15 residues of $A\beta_{42}$.[53] In addition, π–π stacking interaction was observed between Phe19 of $A\beta_{42}$ and Phe4 of KLLFF, with a bond length of 0.4 nm. Additionally, the residues Ser8, Val12, His14, Lys16, Val18, and Phe19 of $A\beta_{42}$ were involved in hydrophobic contacts (Fig. 3b). The docking pose obtained from the molecular docking is further subjected to MD simulations to study the dynamics of $A\beta_{42}$ in presence of KLLFF.

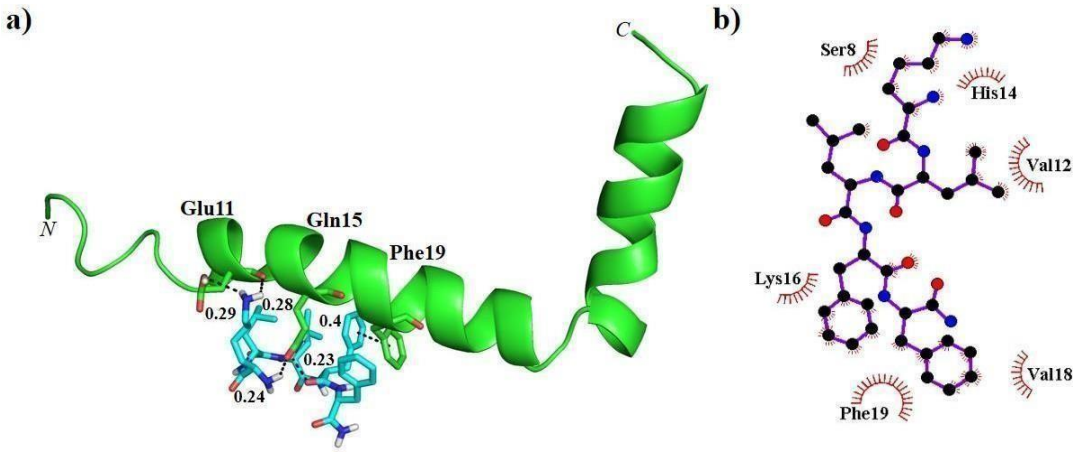

Fig. 8. a) The docked pose of $A\beta_{42}$–KLLFF as viewed in pyMOL showing hydrogen bonds in black dotted lines. b) The 2D interaction map displayed hydrophobic contacts between $A\beta_{42}$ and KLLFF in red semicircles as viewed in Ligplot+.

Table 2. Details of binding interactions between $A\beta_{42}$ and KLLFF.

Complex	Binding affinity (kcal/mol)	Residues and atoms of $A\beta_{42}$ and KLLFF involved in hydrogen bonding		Distance (nm)	Residues of $A\beta_{42}$ involved in hydrophobic contacts with KLLFF
		$A\beta_{42}$	KLLFF		
$A\beta_{42}$–KLLFF	–5.2	Glu11[a] C=O	H–N Lys1[a]	0.29	Ser8, Val12, His14, Lys16, Val18, Phe19
		Glu11[b]C=O	H–N Lys1[a]	0.28	
		Gln15[a]C=O	H–N Lys1[b]	0.24	
		Gln15[a] N–H	O=C Phe4[b]	0.23	

[a]denotes Side chain [b]denotes Main chain

4.2 Structural stability of $A\beta_{42}$ in the presence of KLLFF

The structural stability of $A\beta_{42}$ was evaluated through various analysis like RMSD, RMSF, R_g. The RMSD analysis was conducted for the backbone atoms of both the $A\beta_{42}$ and $A\beta_{42}$–KLLFFto assess the structural deviation of the proteins throughout the MD simulations (Fig. 4a). Initially, $A\beta_{42}$–KLLFF exhibited a higher RMSD compared to $A\beta_{42}$ but over time it attains stability with a lower RMSD value. The average RMSD values for $A\beta_{42}$ and $A\beta_{42}$–KLLFF were noted to be 0.88 ± 0.04 nm and 0.68 ± 0.03 nm, respectively. The reduced average RMSD value implied a more stable structure with lesser overall structural deviations. Further, The RMSF analysis was employed to investigate the fluctuations of C_α atoms of $A\beta_{42}$ residues in the presence and absence of KLLFF. The average RMSF value was 0.56 ± 0.03 for $A\beta_{42}$ and marginally decreased to 0.54 ± 0.03 for $A\beta_{42}$–KLLFF (Fig. 4b). The incorporation of KLLFF resulted inthe reduced fluctuations for the residues Val12, Lys16–Ala21 and Gly37–Gly38 of $A\beta_{42}$. Xu et al. reported reduced fluctuations for residues Leu17–Asn27 and Ala30–Gly37 of $A\beta_{42}$ in the presence of Gallic Acid–Glutamine Conjugate which is relative to our study.[54] This decrease in the RMSF values indicated that the presence of KLLFF led to a reduction in the overall RMSF fluctuations within the $A\beta_{42}$ indicating a stabilizing effect. Additionally, average R_g values noted for $A\beta_{42}$ and for $A\beta_{42}$–KLLFF was 1.27 ± 0.06 and 1.24 ± 0.06, respectively (Fig. 4c). The decrease in the R_g value depicts the compactness and enhanced structural stability of $A\beta_{42}$ in the presence of the KLLFF.

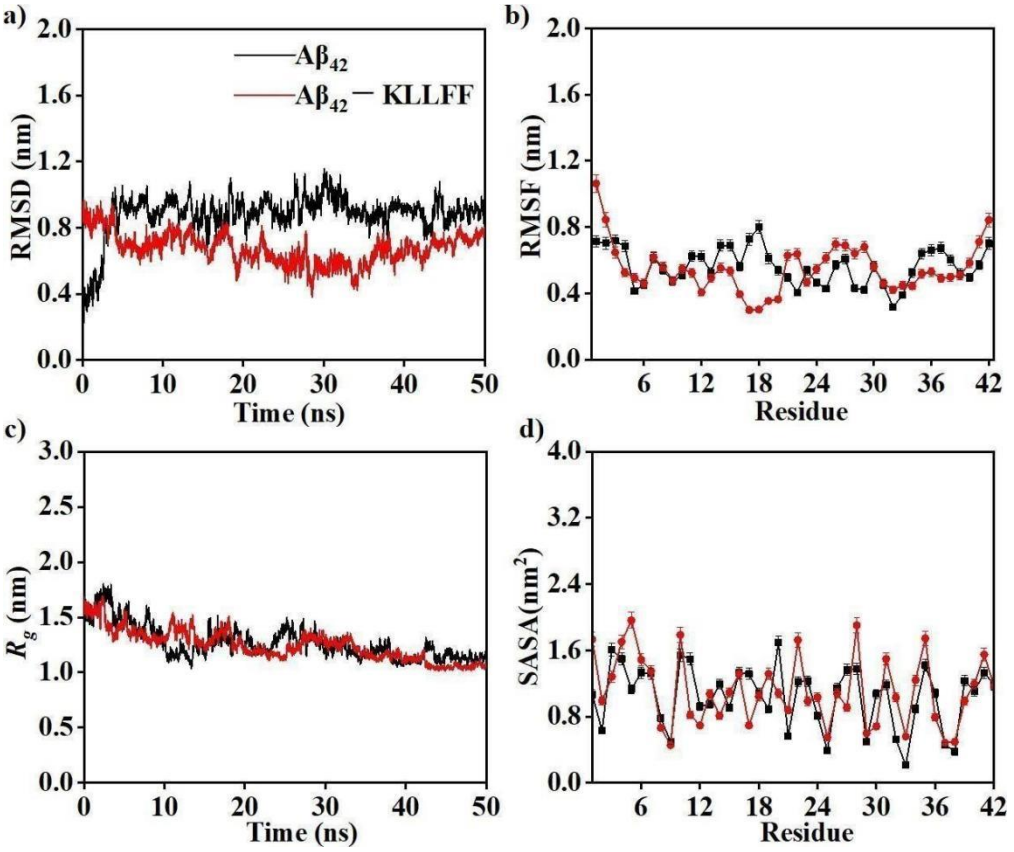

Fig. 9. The analysis of the simulated system Aβ$_{42}$ (black curve) and Aβ$_{42}$–KLLFF (red curve).

a) The RMSD calculated for the backbone atoms of Aβ$_{42}$ b) The RMSF calculated for Cα atomsof Aβ$_{42}$ c) The R_g calculated for the overall size of Aβ$_{42}$ d) SASA calculated for the exposure of the side–chain to solvent molecules.

4.3 Evaluation of SASA for Aβ$_{42}$–KLLFF

The per residue SASA analysis was performed to quantitatively assess the extent of the exposure residues on the surface area of Aβ$_{42}$ to the surrounding solvent molecules (Fig. 4d). By examining the per residue SASA value, notable decrease was observed for the residues Ser8–Gly9, Glu11–Val12, His14, Leu17, Phe20, Asp23, Ser26–Asn27, Ala30, Val36 and Val39 in the presence of KLLFF. The decrease in the SASA value for CHC region highlighted the reduced tendency of Aβ$_{42}$ to aggregate in presence of KLLFF.

4.4 Secondary structure analysis of Aβ$_{42}$ and Aβ$_{42}$–KLLFF

To assess the influence of KLLFF on the secondary structure composition of Aβ$_{42}$, the time–dependent evolution of secondary structure analysis was performed (Fig. 5). In case of Aβ$_{42}$, the predominant secondary structure conformation was helix (34.8%) followed by turn (28%), random coil 22.2%, bend 9.6% and β–sheet 5.8%. In the presence of KLLFF, the random coil confirmation

was the most dominant and increased to 39.2% followed by an increase in bend (22.8%) whereas the helix, turn and β–sheet decreased to 17%, 20.2%, 0.6% respectively. (Table3). The results are consistent with the circular dichroism (CD) and FTIR results which reported a significantreduction in β–sheet and increment in random coil content.[29]

Table 3. Analysis of secondary structure in the absence and presence of KLLFF.

Model System	Coil	Bend	Turn	Helix[a]	β–sheet[b]
$A\beta_{42}$	22.2	9.6	28	34.8	5.8
$A\beta_{42}$–KLLFF	39.2	22.8	20.2	17.0	0.6

[a]Helix is the sum of α –, π – and 3_{10}–helix; [b]β–sheet is the sum of β–bridge and β–sheet.

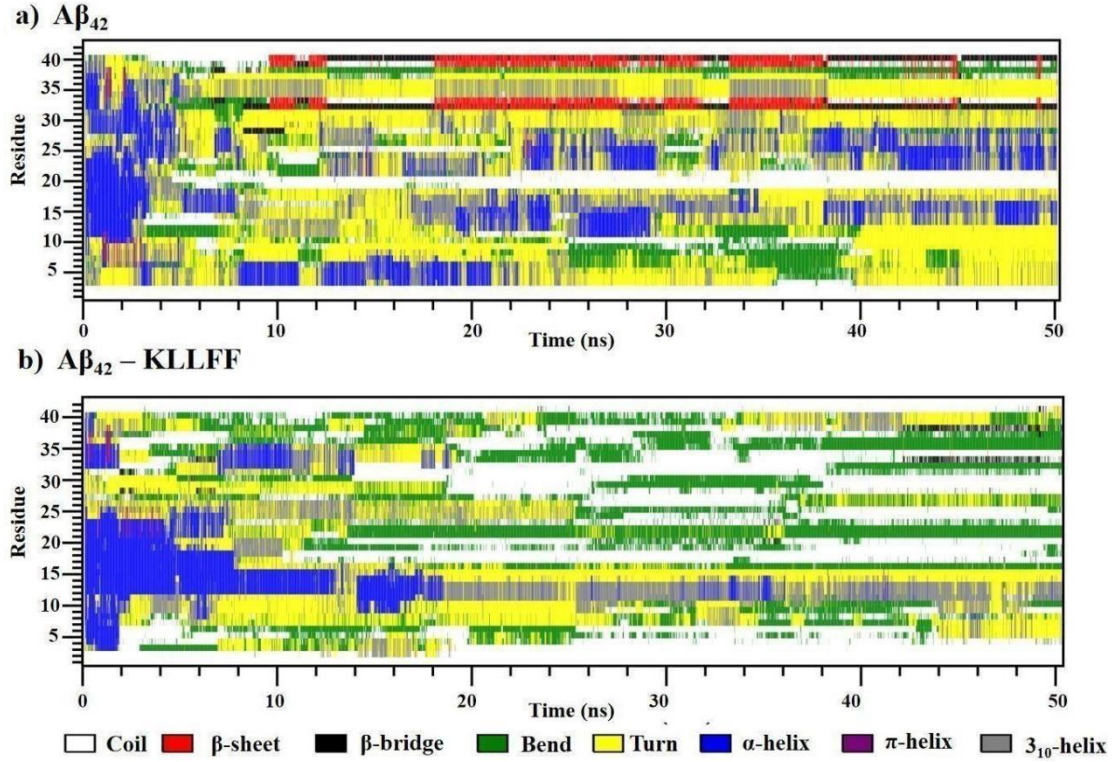

Fig. 10. The time dependent secondary structure analysis for $A\beta_{42}$. a) in the absence b) in thepresence of KLLFF as calculated by DSSP.

The per residue secondary structure analysis was performed to get a deeper insight into the secondary structural preferences of each residue of $A\beta_{42}$ in the absence and presence of KLLFF (Fig. 6). Coil conformation increased remarkably for Ala2, Glu11 and Leu17–Ser26 residuesof $A\beta_{42}$ in the presence of KLLFF (Fig. 6a). The increase in the coil conformation for $A\beta_{42}$–KLLFF plays a key role in inhibiting the aggregation of $A\beta_{42}$ is consistent with experimental studies. Bora et al. reported an increase in the coil for the residues Gln15–Leu17 and Asn17– Gly29 for $A\beta_{42,}$ which is consistent with our results.[55] In the presence of KLLFF, the bend confirmation increased

significantly for the residues Phe4, Tyr10, His13–Leu17, Phe19– Ala21, Asp23–Ile31, andGly33–Leu34 (Fig. 6b). However, decrease in turn was evident for the residuesGlu3, Arg5–Asp7,Glu11–Val12, Lys16–Val18, Ala21, Asp23–Gly25, and Lys28–Ile31 of $A\beta_{42}$ (Fig 6c). The decrease in the helix was observed for the residues Asp1– Ala2, Ser8–Gly25, Lys28–le31, Met35–Ala42 showed a decrease in the helix whereas for residues Glu3–Asp7, Ser26–Asn27and Ile32– Gly34 there was an increase in the helix content (Fig. 6d). The residues that showed significant decrease in β–sheet included Glu22, Ser26–Asn27 and Gly33–Leu34 (Fig.6e). Previous studies have shown that residue Val24–Val40 are essential for β–sheet formation.[56] The presence of β– sheet is responsible for the aggregation of $A\beta_{42}$ and decrease in β–sheet content indicates inhibitionof aggregation.[57] The decrease in the β–sheet content in the presence of KLLFF clearly indicated theaggregation was inhibited in the presence of KLLFF.

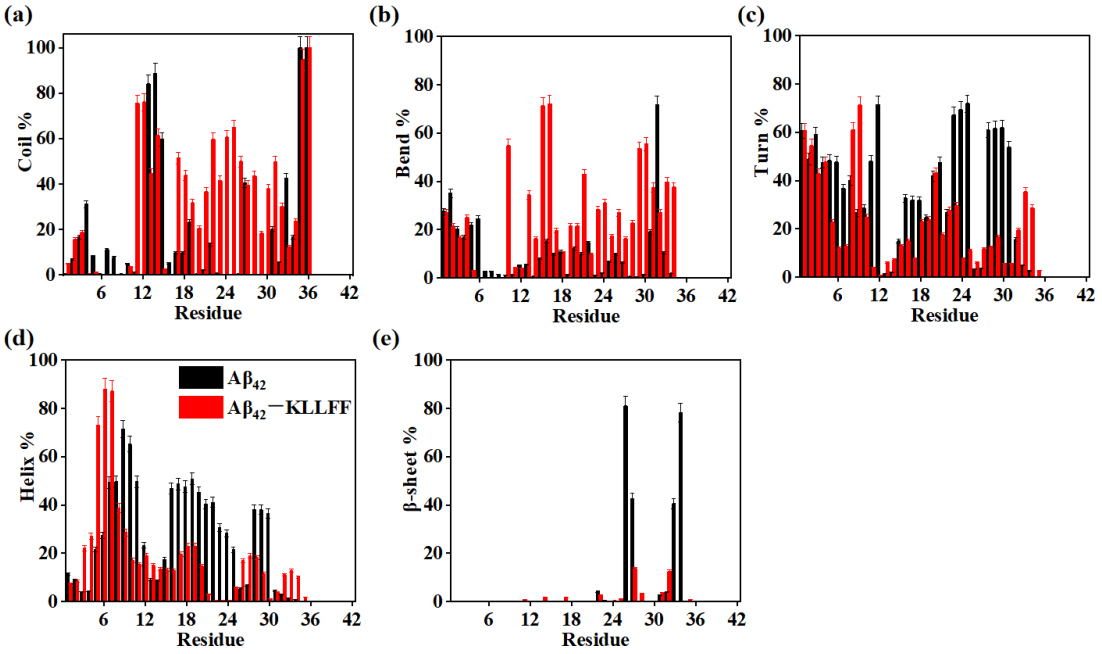

Fig. 11. The per residue secondary structure analysis exhibiting the distribution of (a) Coil (b) Bend (c) Turn (d) Helix (e) β–sheet content as calculated for $A\beta_{42}$ in the absence (black bars) and presence of KLLFF (red bars).

In addition, snapshots of both the systems at different time scales have also been compared to verify the structural changes of $A\beta_{42}$ in the absence and presence of KLLFF. The snapshots were taken at an interval of every 10 ns throughout the trajectory for both the system as shownin (Fig. 7). A notable transformation in the conformation of $A\beta_{42}$, exhibiting a considerable decrease in helix content was observed (Fig. 7a). The snapshots of $A\beta_{42}$ in the presence of KLLFF illustrates that the random coil conformation has increased significantly for $A\beta_{42}$ (Fig.7b). Moreover, the KLLFF remains bound to $A\beta_{42}$ throughout the simulation. The increase in coil content for $A\beta_{42}$–

KLLFF system is consistent with the secondary structure details in whichcoil content increased to 39.20%.

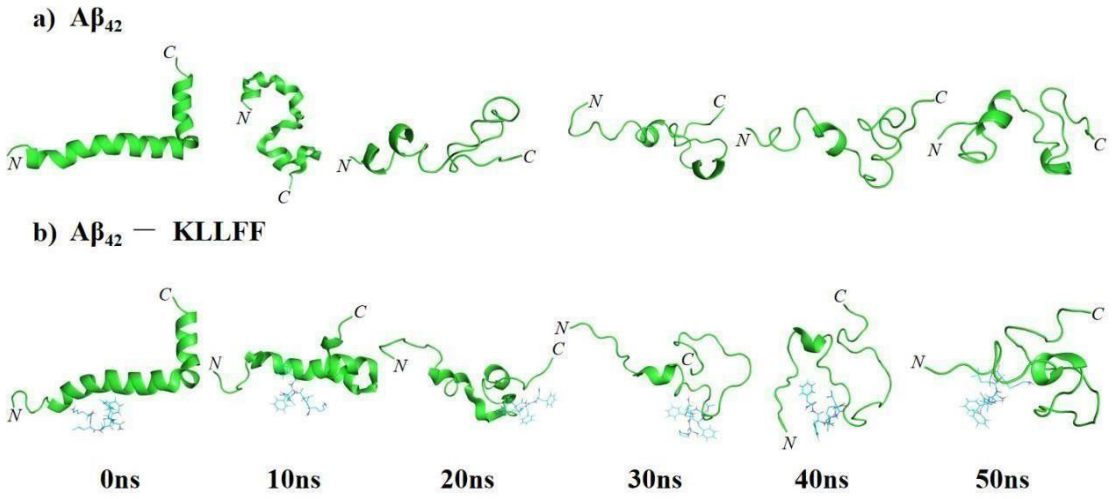

Fig. 12. The snapshots extracted after every 10 ns from MD simulation trajectory for both the systems.

4.5 Hydrogen Bond Analysis

The investigation focused on exploring the impact of Aβ42 on both intramolecular and intermolecular hydrogen bonds in the absence and presence of KLLFF. The average number of intramolecular hydrogen bonds was 21.00 ± 1.08 for Aβ42 and 17.00 ± 0.84 Aβ42–KLLFF (Fig. 8a). The presence of KLLFF leads to a decrease in average number of intramolecular hydrogen bonds within Aβ42 which indicates the critical role of KLLFF in modulating the secondary structure of Aβ42. The average number of intermolecular hydrogen bonds between Aβ42 and KLLFF was calculated to be 1.20 ± 0.06 (Fig. 8b) depicting that KLLFF remains in the vicinity of Aβ42 throughout the simulation.

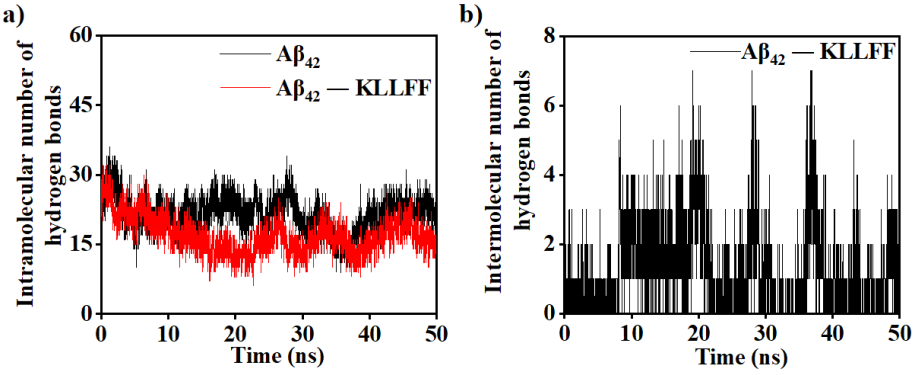

Fig. 13. a) The number of intramolecular hydrogen bonds between formed by Aβ42 in the presence and absence of the peptide. b) The number of intermolecular hydrogen bonds between Aβ42 and KLLFF.

4.6 The influence of KLLFF on tertiary contacts between $A\beta_{42}$

The side chain–side chain contacts of $A\beta_{42}$ and $A\beta_{42}$–KLLFF was analyzed. For $A\beta_{42}$ considerable contacts within the residues Gly33–Val40 (Fig. 9a) were observed. However, the introduction of KLLFF vividly portrays considerable reduction in the contacts within the residues Gly33–Val40 region (Fig. 9b). The reduction strongly suggests a decrease in the β–sheet. Theinteractions between CHC and C–terminal regions play an important role in the self–aggregation of $A\beta_{42}$.[58] The findings illustrate that the presence of KLLFF influences the structural characteristicsof $A\beta_{42}$ by diminishing the side chain–side chain contacts within the residues Gly33–Val40.

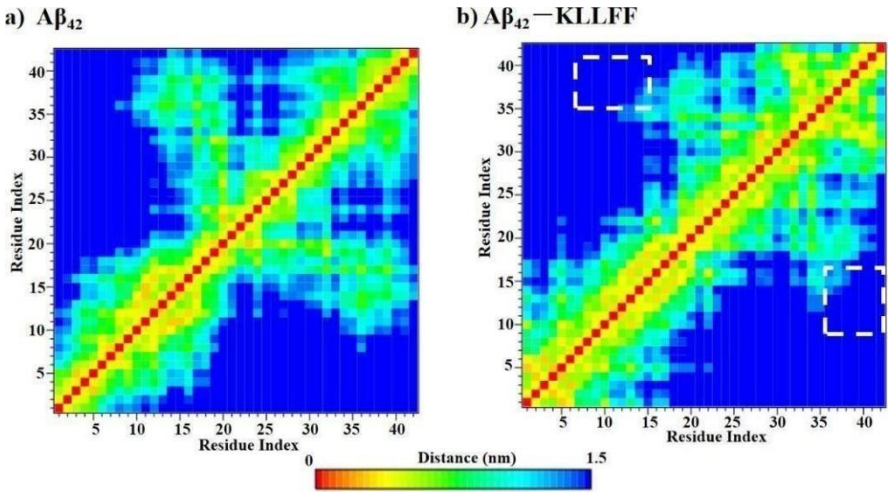

Fig. 14 The color–coded contact map represents the interactions between the side chain atoms of $A\beta_{42}$. In this representation, different colors indicate the frequency of contacts between the atoms,with darker colors representing stronger interactions.

4.7 Binding free energy analysis between $A\beta_{42}$ and KLLFF

The binding free energy calculation depicted binding free energy ($\Delta G_{binding}$) value to be –26.21 ± 5.16 kcal/mol between $A\beta_{42}$ and KLLFF (Fig. 10b). The vander Waals energy was observed to be the dominating with value of –24.03 ± 9.81 kcal/mol. The per–residue energy decomposition evaluated the contribution of individual residues of $A\beta_{42}$ revealing valuable insights into the molecular interactions driving the binding free energy. Notably,the residues exhibiting the binding energy less than –1.0 kcal/mol have been identified as important contributors for binding. The six residues Phe4, Arg5, Val12, His13, Val18, and Phe19 of $A\beta_{42}$ contributed the most to the binding with KLLFF (Fig.10a). The result agrees with the previous studies which state that the residues Val24–Ala42 adopts β–sheet conformation and the residues of N–terminal Tyr10–Val24[59] affect the rate of β–sheet formation. Thus, the binding energy of CHC residues, Val12, Val18 and Val19 to KLLFF highlighted the decreased aggregationpropensity of $A\beta_{42}$ could be in presence of KLLFF.

a)

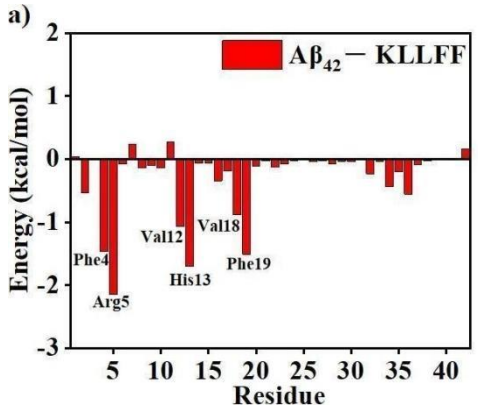

b)

Energy terms	$A\beta_{42}$– KLLFF
ΔE_{vdW}	–24.03 ± 9.81
ΔE_{elec}	–4.49 ± 2.60
ΔE_{MM} [a]	–28.52 ± 7.21
ΔG_{ps}	5.83 ± 3.24
ΔG_{nps}	–3.52 ± 1.19
ΔG_{solv} [b]	2.31 ± 2.05
$\Delta G_{binding}$ [c]	–26.21 ± 5.16

[a] $\Delta E_{MM} = \Delta E_{vdW} + \Delta Eelec$;
[b] $\Delta G_{solv} = \Delta G_{ps} + \Delta Gnps$;
[c] $\Delta G_{binding} = \Delta E_{MM} + \Delta G_{solv}$

Fig. 15. (a) The energy contribution of each residue in the $A\beta_{42}$–KLLFF system. (b) This table depicts the computed binding free energy along with the individual contributions of molecular mechanics interactions, solvation terms.

CHAPTER 5: Conclusion

In the present study, the inhibitory mechanism of KLLFF against $A\beta_{42}$ aggregation was investigated by performing the MD simulations. MD studies revealed that KLLFF inhibited the β–sheet formation. KLLFF formed hydrogen bonds with Glu11 and Gln15 of $A\beta_{42}$ while the residues Ser8, Val12, His14, Lys16, Val18 and Phe19 were involved in the hydrophobic interactions. The RMSD, RMSF and R_g analyses revealed enhanced structural stability with the incorporation of KLLFF. The presence of $A\beta_{42}$ increased the coil content to 39.2% and completely diminished the β–sheet. A reduction in intramolecular hydrogen bonds further confirmed that KLLFF has increased the stability of $A\beta_{42}$ and has reduced the aggregation. The side chain contact maps revealed that the contacts in the C–terminal, responsible for the formation of β–sheet have decreased indicating the reduction in the $A\beta_{42}$ aggregation and subsequent β–sheet formation. MD simulations depicted that KLLFF inhibited $A\beta_{42}$ aggregation by blocking the conformational transition of $A\beta_{42}$ monomer. The study provides insight into the inhibition mechanism of KLLFF against $A\beta_{42}$ aggregation.

References

1. Chandel, T. I.; Zaman, M.; Khan, M. V.; Ali, M.; Rabbani, G.; Ishtikhar, M.; Khan, R. H. A mechanistic insight into protein–ligand interaction, folding, misfolding, aggregation and inhibition of protein aggregates: An overview. *Int. J. Biol. Macromol.* **2018**, *106*, 1115–1129.
2. Ellis, R. J.; Pinheiro, T. J. Danger-misfolding proteins. *Nature* **2002**, *416*, 483–484.
3. Hartl, F. U. Protein misfolding diseases. *Ann Rev Biochem.***2017**, *86*, 21–26.
4. Nguyen, P. H.; Ramamoorthy, A.; Sahoo, B. R.; Zheng, J.; Faller, P.; Straub, J. E.; Dominguez, L.; Shea, J.–E.; Dokholyan, N. V.; De Simone, A.; Ma, B.; Nussinov, R.; Najafi, S.; Ngo, S. T.; Loquet, A.; Chiricotto, M.; Ganguly, P.; McCarty, J.; Li, M. S.; Hall, C.; Wang, Y.; Miller, Y.; Melchionna, S.; Habenstein, B.; Timr, S.; Chen, J.; Hnath, B.; Strodel, B.; Kayed, R.; Lesne´, S.; Wei, G.; Sterpone, F.; Doig, A. J.; Derreumaux, P. Amyloid oligomers: A joint experimental/computational perspective on Alzheimer's disease, Parkinson's disease, Type II diabetes and Amyotrophic Lateral Sclerosis. *Chem. Rev*. **2021**, *121*, 2545–2647.
5. Soto, C.; Pritzkow, S. Protein misfolding, aggregation, and conformational strains in neurodegenerative diseases. *Nat. Neurosci.* **2018**, *21*, 1332–1340.
6. Hardy, J; Selkoe, D. J. The amyloid hypothesis of Alzheimer's disease: Progress and problems on the road to therapeutics. *Science* **2002**, *297*, 353–356.
7. (a) Goedert, M.; Spillantini, M. G. A Century of Alzheimer's disease. *Science* **2006**, *314*, 777–781. (b) Alzheimer, A.; Über Eine Eigenartige Erkrankung Der Hirnrinde. *Allg. Zschr.Psychiat. Psych. gerichtl. Med*. **1907**, *64*, 146–148.
8. Alzheimer's Association 2022. Alzheimer's disease facts and figures. *Alzheimer's Demen*. **2022**, 18, 700–789.
9. https://www.alzint.org/about/dementia–facts–figures/dementia–statistics/.
10. Ono, K. Alzheimer's disease as oligomeropathy. *Neurochem. Int*. **2018**, *119*, 57–70.
11. Clippingdale, A. B.; Wade, J. D.; Barrow C. J. The Amyloid-β peptide and its role in Alzheimer's disease. *J. Pept. Sci.* **2001**, *7*, 227–249.
12. Mattson, M. P. Cellular actions of beta-amyloid precursor protein and its soluble and fibrillogenic derivatives. *Physiol. Rev*. **1997**, *77*, 1081–1132.
13. Yan, R.; Vassar, R. Targeting the β–Secretase BACE1 for Alzheimer's disease therapy. *Lancet Neurol.* **2014**, *13*, 319–329.
14. Kaffy, J.; Brinet D.; J. L.; Correia, I.; Tonali, N.; Fera, K.F.; Iacone, Y.; Hoffmann, A. R.; Khemtémourian, L.; Crousse B.; Taylor, M.; Designed glycopeptidomimetics disrupt

protein–protein interactions mediating amyloid β–peptide aggregation and restore neuroblastoma cell viability. *J. Med. Chem*. **2016**, *59*, 2025–2040.

15. Ahmed, M.; Davis, J.; Aucoin, D.; Sato, T.; Ahuja, S.; Aimoto, S.; Elliott, J. I.; Van Nostrand, W. E.; Smith, S. O. Structural conversion of neurotoxic amyloid–β1–42 oligomers to fibrils. *Nat. Struct. Mol. Biol*. **2010**, *17*, 561–567.

16. Chen, Y.; Li, X.; Zhan, C.; Lao, Z.; Li, F.; Dong, X.; Wei, G. A comprehensive insight into the mechanisms of dopamine in disrupting Aβ protofibrils and inhibiting Aβ aggregation. ACS *Chem. Neurosci.* **2021**, *12*, 4007–4019.

17. Fan, H.-M.; Gu, R.-X.; Y.-J.; Zhang, Y.-H.; Xu, Q.; Wei, D.-Q. Destabilization of Alzheimer's Aβ42 protofibrils with a novel drug candidate wgx–50 by molecular dynamics simulations. *J. Phys. Chem. B.* **2015**, *119*, 11196–11202.

18. Takahashi, T.; Mihara, H. Peptide and protein mimetics inhibiting amyloid-beta peptide aggregation. *Acc. Chem. Res.* **2008**, *41*, 1309–1318.

19. He, C. Q.; Han, Y. C.; Zhu, L. Y.; Deng, M. L.; Wang, Y. L. Modulation of Aβ(1-40) peptide fibrillar architectures by Aβ-based peptide amphiphiles. *J. Phys. Chem. B.* **2013**, *117*, 10475–10483.

20. Amijee, H.; Middleton, D. A.; Doig. A. J. Inhibitors of protein aggregation and toxicity. *Biochem. Soc. Trans.* **2009**, *37*, 692–696.

21. Cabaleiro-Lago, C.; Quinlan–Pluck, F.; Lynch, I.; Lindman, S.; Minogue, A. M.; Thulin, E.; Walsh, D. M.; Dawson, K. A.; Linse, S. Inhibition of amyloid β protein fibrillation by polymeric nanoparticles. *J. Am. Chem. Soc.* **2008**, *130*, 15437–15443.

22. Dash, P. K.; Moore, A. N.; Orsi, S. A. Blockade of γ-secretase activity within the hippocampus enhances long-term memory. *Biochem. Biophys. Res. Commun.* **2005**, *338*, 777–782.

23. (a) Asai, M.; Hattori, C.; Iwata, N.; Saido, T. C.; Sasagawa, N.; Szabo, B.; Hashimoto, Y.; Maruyama, K.; Tanuma, S.; Kiso, Y.; Ishiura, S. The novel β-secretase inhibitor KMI-429 reduces amyloid β peptide production in amyloid precursor protein transgenic and wild-type mice. *J. Neurochem.* **2006**, *96*, 533–540. (b) Backskai, B. J.; Kajdasz, S. T.; Christie, R. H.; Carter, C.; Games, D.; Seubert, P.; Schenk, D.; Hyman, B. T. Imaging of amyloid-β deposits in brains of living mice permits direct observation of clearance of plaques with immunotherapy. *Nat. Med.* **2001**, *7*, 369–372.

24. Kanchi, P. K.; Dasmahapatra, A. K. Destabilization of the Alzheimer's amyloid–β peptide by a proline–rich β–sheet breaker peptide: A molecular dynamics simulation study. *J. Mol. Model.* **2021**, *27*, 1–5.

25. Goyal, D.; Shuaib, S.; Mann, S.; Goyal, B. Rationally designed peptides and peptidomimetics as inhibitors of amyloid-β (Aβ) aggregation: potential therapeutics of

Alzheimer's disease. *ACS Comb. Sci*. **2017**, *19*, 55–80.

26. Liu, J.; Wang, W.; Zhang, Q.; Zhang, S.; Yuan, Z. Study on the efficiency and interaction mechanism of a decapeptide inhibitor of β-amyloid aggregation. *Biomacromolecules* **2014**, *15*, 931–939.

27. (a) Tjernberg, L. O.; Näslund, J.; Lindqvist, F.; Johansson, J.; Karlstrom, A. R.; Thyberg, J.; Terenius, L.; and Nordstedt, C. Arrest of β–amyloid fibril formation by a pentapeptide ligand. *J. Biol. Chem.* **1996**, *271*, 8545–8548. (b) Shuaib, S.; Narang, S. S.; Goyal, D.; Goyal, B. Computational design, and evaluation of β-sheet breaker peptides for destabilizing Alzheimer's amyloid-β_{42} protofibrils. *J. Cell. Biochem.* **2019**, *120*, 17935–17950.

28. Rafferty, J.; Nagaraj, H.; McCloskey, A. P.; Huwaitat, R.; Porter, S.; Albadr, A.; Laverty, G. Peptide therapeutics and the pharmaceutical industry: barriers encountered translating from the laboratory to patients. *Curr. Med. Chem.* **2016**, *23*, 4231–4259.

29. Mallesh, R.; Juhee Khan; Gharai, P.K.; Gupta, V.; Roy, R.; Ghosh, S. Controlling amyloid–β peptide aggregation and toxicity by protease–stable ligands. *ACS Bio. Med. Chem. Au* **2023**, *3*, 158–173.

30. Konar, M.; Ghosh, D.; Samanta, S.; Govindaraju, T. Combating amyloid–induced cellular toxicity and stiffness by designer peptidomimetics. *RSC Chem. Biol.* **2022**, *3*,220–226.

31. Kundal, K.; Paramasivam, S.; Mitra, A.; Sarkar, N. In silico identification of novelpeptides as potential modulators of $A\beta_{42}$ amyloidogenesis. *bioRxiv* **2022**, 2022–2049.

32. Liu, W.; Sun, X.; Dong, X.; Sun, Y. Chiral LVFFARK enantioselectively inhibitsamyloid–β protein fibrillogenesis. *Chin. J. Chem. Eng*. **2022**, *48*, 227–235.

33. Wang, W.; Zhao, G.; Dong, X.; Sun, Y.Unexpected function of a heptapeptide–conjugated zwitterionic polymer that co assembles into β-amyloid fibrils and eliminates the amyloid cytotoxicity. *ACS Appl. Mater. Interfaces* **2021**, *13*, 18089-18099.

34. Horsley, J. R.; Jovcevski, B.; Wegener, K. L.; Yu, J.; Pukala, T. L.; Abell, A. D. Rationally designed peptide–based inhibitor of Aβ42 fibril formation and toxicity: A potential therapeutic strategy for Alzheimer's disease. *Biochem. J*. **2020**, *477*, 2039–2054.

35. Mondal, P.; Khan, J.; Gupta, V.; Ghosh, S. In silico approach for designing potent neuroprotective hexapeptide. *ACS Chem. Neurosci.* **2019**, *10*, 3018–3030.

36. Crescenzi, O.; Tomaselli, S.; Guerrini, R.; Salvadori, S.; D'Ursi, A. M.; Temussi, P. A.; Picone, D. Solution structure of the Alzheimer amyloid β–peptide (1–42) in a polar microenvironment: Similarity with a virus fusion domain. *Eur. J. Biochem.* **2002**, *269*, 5642–5648.

37. Zardecki, C.; Dutta, S.; Goodsell, D. S.; Voigt, M.; & Burley, S. K. RCSB Protein Data Bank: A resource for chemical, biochemical, and structural explorations of large and small

biomolecules. *J. Chem. Educ.* **2016**, 93, 569–575.

38. Mills, N. ChemDraw Ultra 10.0. *J. Am. Chem. Soc.* **2006**, *128*, 13649–13650.
39. Morris, G. M.; Goodsell, D. S.; Halliday, R. S.; Huey, R.; Hart, W. E.; Belew, R. K.; Olson, A. J. Automated docking using a Lamarckian genetic algorithm and an empirical binding free energy function. *J. comput.chem.* **1998**, *19*, 1639-1662.
40. Trott, O.; Olson, A.J. AutoDock Vina: Improving the speed and accuracy of dockingwith a new scoring function, efficient optimization and multithreading. *J. Comput. Chem.* **2010**, *31*, 455–461.
41. (a) R. A. Laskowski and M. B. Swindells, LigPlot+: Multiple ligand-protein interaction diagrams for drug discovery. *J. Chem. Inf. Model.*, **2011**, *51*, 2778–2786; (b) W. L. DeLano, The PyMOL molecular graphics system. *571*, DeLano Scientific, San Carlos, CA. **2002**.
42. Hansson, T.; Oostenbrink, C.; van Gunsteren, W. Molecular dynamics simulations. *Curr. Opin. Struct. Biol.* **2002**, *12*, 190–196.
43. Abraham, M.J.; Murtola, T.; Schulz, R.; Páll, S.; Smith, J.C.; Hess, B.; Lindahl, E.; GROMACS: High performance molecular simulations through multi-level parallelism from laptops to supercomputers. *SoftwareX* **2015**, *1*, 19–25.
44. Smith, M. D.; Rao, J. S.; Segelken, E.; Cruz, L. Force–field induced bias in the structure of $A\beta_{21–30}$: A Comparison of OPLS, AMBER, CHARMM, and GROMOS force fields. *J. Chem. Inf. Model*. 2015, *55*, 2587–2595.
45. Mark, P.; Nilsson, L. Structure and dynamics of the TIP3P, SPC, and SPC/E water models at 298 K. *J. Phys. Chem. A.* **2001**, *10*, 9954–9960.
46. Baumketner, A.; Bernstein, S. L.; Wyttenbach, T.; Bitan, G.; Teplow, D. B.; Bowers, M. T.; Shea, J. E. Amyloid β-protein monomer structure: A computational and experimental study. *Protein Sci*. **2006**, *15*, 420–428.
47. Berendsen, H. J.; Postma, J. V.; Van Gunsteren, W. F.; DiNola, A. R. H. J.; Haak, J. R. Molecular dynamics with coupling to an external bath. *J. Chem. Phys.* **1984**, *81*, 3684–3690.
48. Parrinello, M.; Rahman, A. Polymorphic transitions in single crystals: A new molecular dynamics method. *J. Appl. Phys.* **1981**, *52*, 7182–7190.
49. Hess, B.; Bekker, H.; Berendsen, H. J.; Fraaije, J. G. LINCS: A linear constraint solver for molecular simulations. *J. Comput. Chem.* **1997**, *18*, 1463–1472.
50. Essmann, U.; Perera, L.; Berkowitz, M. L.; Darden, T.; Lee, H.; Pedersen, L. G. A smooth particle mesh Ewald method. *J. Chem. Phys.* **1995**, *103*, 8577–8593.
51. Kabsch, W.; Sander, C. Dictionary of protein secondary structure: Pattern recognition of hydrogen-bonded and geometrical features. *Biopolymers* **1983**, *22*, 2577–2637.
52. Kumari, R.; Kumar, R. g_mmpbsa—A GROMACS tool for high–throughput MM–PBSA

calculations. *J. Chem. Inf. Model.* **2014**, *54*, 1951–1962.

53. Biswas, A.; Kurkute, P.; Saleem, S.; Jana, B.; Mohapatra, S.; Mondal, P.; Adak, A.; Ghosh, S.; Saha, A.; Bhunia, D.; Biswas, S. C.; Ghosh, S. Novel hexapeptide interacts with tubulin and microtubules, inhibits Aβ fibrillation, and shows significant neuroprotection. *ACS Chem. Neurosci.* **2015**, *6*, 1309–1316.

54. Xu, S.; Sun, Y.; Dong, X. Design of gallic acid–glutamine conjugate and chemical implications for its potency against Alzheimer's amyloid–β fibrillogenesis. *Bioconjug. Chem*. **2022**, *33*, 677–690.

55. Bora, R. P.; Prabhakar, R. Elucidation of interactions of Alzheimer amyloid β peptides (Aβ40 and Aβ42) with insulin degrading enzyme: a molecular dynamics study. *Biochemistry* **2010**, *49*, 3947–3956.

56. Xu, Y.; Shen, J.; Luo, X.; Zhu, W.; Chen, K.; Ma, J.; Jiang, H. Conformational transition of amyloid β peptide. *Proc. Natl. Acad. Sci. U. S. A* **2005**, *102*, 5403–5407.

57. (a) Bartolini, M.; Bertucci, C.; Bolognesi, M. L.; Cavalli, A.; Melchiorre, C.; Andrisano, V. Insight into the kinetic of amyloid β. *Chembiochem* **2007**, *8*, 2152–2161. (b) Takahashi, T.; Mihara, H. Peptide and protein mimetics inhibiting amyloid β peptide aggregation. *Acc. Chem. Res.* **2008**, *41*, 1309–1318. (c) Viet, M. H.; Ngo, S. T.; Lam, N. S.; Li, M. S. Inhibition of aggregation of amyloid peptides by β–sheet breaker peptides and their binding affinity. *J. Phys. Chem. B* **2011**, *115*, 7433–7446.

58. (a) Yang, M.; Teplow, D. B. Amyloid β–protein monomer folding: free energy surfaces reveal alloform specific differences. *J. Mol. Biol*. **2008**, *384*, 450–464. (b) Urbanc, B.; Cruz, L.; Yun, S.; Buldyrev, S. V.; Bitan, G.; Teplow, D. B.; Stanley, H. E. In silico study of amyloid β protein folding and oligomerization. *Proc. Natl. Acad. Sci. U.S.A* **2004**, *101*, 17345–17350 (c) Coskuner, O.; Wise–Scira, O. Arginine and disordered amyloid β peptide structures: Molecular level insights into the toxicity in Alzheimer's disease. *ACS Chem. Neurosci.* **2013**, *4*, 1549–1558.

59. Pike, C. J.; Walencewicz-Wasserman, A. J.; Kosmoski, J.; Cribbs, D. H.; Glabe, C. G.; Cotman, C. W. Structure-activity analyses of β-amyloid peptides: contributions of the β25–35 region to aggregation and neurotoxicity. *J. Neurochem*. **1995**, *64*, 253–265.

Document Information

Analyzed document	msc-maw.docx (D172423424)
Submitted	7/28/2023 8:23:00 AM
Submitted by	
Submitter email	bhupesh@thapar.edu
Similarity	2%
Analysis address	bhupesh.thapar@analysis.urkund.com

Sources included in the report

SA **MANUSCRIPT.doc** 1
Document MANUSCRIPT.doc (D32891293)

SA **JIBIN K VARUGHESE-A COMPUTATIONAL CHEMISTRY INVESTIGATION ON THE BINDING AND INHIBITORY ACTIVITY OF SOME SELECTED FLAVONOIDS AGAINST SARS VIRAL TARGET PROTEINS.pdf** 1
Document JIBIN K VARUGHESE-A COMPUTATIONAL CHEMISTRY INVESTIGATION ON THE BINDING AND INHIBITORY ACTIVITY OF SOME SELECTED FLAVONOIDS AGAINST SARS VIRAL TARGET PROTEINS.pdf (D172405999)

SA **Thapar Institute Of Engineering And Technology / Dessertation-Smriti-urkund.docx** 4
Document Dessertation-Smriti-urkund.docx (D142386833)
Submitted by: bhupesh@thapar.edu
Receiver: bhupesh.thapar@analysis.urkund.com

Entire Document

ABSTRACT

The self–aggregation of amyloid-β (Aβ42) into β–sheets is considered to be responsible for the onset of Alzheimer's Disease (AD), a neurodegenerative disease with no clinically accepted treatment. The N–terminal (16KLVFF20) is identified as a self–recognition region and the central hydrophobic core (CHC) which is crucial for the formation and stabilization of the β–sheets. Mallesh et al. have recently reported KLLFF, produced by single point mutation by replacing Val18 in KLVFF with leucine KLLFF as a potential inhibitor against Aβ aggregation. The mechanism by which KLLFF hinders Aβ aggregation remains an enigma. To gain insights into this inhibitory mechanism, molecular dynamics (MD) simulations have been performed. The molecular docking was performed using AutoDock Vina which predicted a favourable binding energy of –5.2 kcal/mol for Aβ42–KLLFF complex. The MD simulations depicted enhanced structural stability for Aβ42 in the presence of KLLFF. The presence of KLLFF remarkably prevented the β–sheet formation by reducing the side–chain contacts at the C–terminal, Gly33–Val40 of Aβ42. According to the per residue binding energy Phe4, Arg5, Val12, His13, Val18 and Phe19 contributed maximum to binding of Aβ42 with KLLFF. KLLFF further reduced the intramolecular hydrogen bonds of Aβ42, thereby stabilizing the native of structure Aβ42. Understanding the inhibitory mechanism of KLLFF against Aβ42 holds great promise for the development of potent drugs to combat AD. Such insights could pave the way for more effective treatments against AD.

CHAPTER 1: Introduction

1. Introduction

Bhupesh Goyal
28/7/23